

# FLOW NEAR GROIN-LIKE STRUCTURES

By Nallamuthu Rajaratnam,<sup>1</sup> M. ASCE  
and Benjamin A. Nwachukwu<sup>2</sup>

**ABSTRACT:** This paper presents the results of an experimental study on the structure of turbulent flow near groin-like structures. Based on experimental observations, the deflected flow has been analyzed using the model of the three-dimensional turbulent boundary layer. The flow bounded by the separating stream line, the groin, and the adjacent bank has been analyzed by treating it as a shear layer in which the velocity profiles have been found to be similar. The amplified bed shear stress near the groin has also been analyzed using the similarity idea. Even though the majority of the present experiments were done with the thin-plate groin, some observations were also made on a groin with a semicylindrical nose.

## INTRODUCTION

Groines are structures used in rivers to protect banks from erosion caused by flow concentration and attack and also to divert or guide the flow. Even though many experimental studies have been performed to observe the erosion near groines and express the results in dimensionless forms, thereby developing empirical methods of predicting scour in the vicinity of groines (1,2,4), comparatively very little work appears to have been done to understand the nature and structure of the turbulent flow near groynes (3,16). It appears that this understanding of the nature of flow will help develop not only more general methods of predicting the erosion around groines but also will throw more light on the flow and erosion around other related structures like piers and abutments. In this project, which is exploratory and experimental in nature, the characteristics of the time-averaged turbulent flow, near (mostly) thin plate groines projecting perpendicularly into a fully developed turbulent flow in a long rectangular channel, have been studied, and the results are presented in this paper. The study has been extended to ob-

<sup>1</sup>Prof., Dept. of Civ. Engrg., Univ. of Alberta, Edmonton, Alberta, Canada.

<sup>2</sup>Office of the Resident Engr., Aba New Water Supply Project, Aba, Nigeria; formerly Grad. Student, Dept. of Civil Engrg., Univ. of Alberta, Edmonton, Canada.

Note.—Discussion open until August 1, 1983. To extend the closing date one month, a written request must be filed with the ASCE Manager of Technical and Professional Publications. The manuscript for this paper was submitted for review and possible publication on August 5, 1980. This paper is part of the *Journal of Hydraulic Engineering*, Vol. 109, No. 3, March, 1983. ©ASCE, ISSN 0733-9429/83/0003-0463/\$01.00. Proc. No. 17792.

serve the erosion process near a groin, and these results will be published later.

## EXPERIMENTAL ARRANGEMENT AND EXPERIMENTS

The experiments were conducted in a straight tilting rectangular flume, 120 ft (37 m) long, 3 ft (0.92 m) wide and 2.5 ft (0.76 m) deep with smooth bed and sides. The test reach was located in the downstream half of the flume. At the downstream end of the flume, a tail gate was installed to regulate the depth of flow. Water was pumped from an underlying sump into the flume head tank through a 12-in. (0.31 m) diameter pipe. The flow was measured with an 8-in. (0.20-m) Foxboro magnetic flow meter.

Most of the testing was done with a smooth bed. To determine the effect of roughness, some runs were made with the bed covered with two types of prefabricated uniform roughness. These were (1) Number 36 aluminum oxide wet-or-dry cloth manufactured by the 3M Company, for which the mean grain size has been found (5) to be 0.56 mm; (2) closely packed 1/2-in. (12.7-mm) diam hemispheres molded from hard rubber into rectangular sheets, for which the roughness height is 6.3 mm.

The groin used for most of this study was an aluminum plate of thickness of 3 mm and projection lengths,  $b$ , of 6 in. and 3 in. (152 mm and 76 mm), respectively, and each had a large enough height to project well above the water surface. Two experiments were done with a groin which was semicylindrical in section with a radius of 6 in. (152 mm).

Flow velocities were measured with a Prandtl-type pitot-static tube of 3-mm external diam, in regions of undisturbed (or parallel) channel flow. But in regions in which the flow was skewed, a three-tube yaw probe was used. This yaw probe was made of three lengths of stainless steel tubing of 3-mm outer diam and 1.8-mm inner diameter, rigidly soldered together. The center tube had a flat nose, while the side tubes were chamfered at an angle of 45°.

In the undisturbed uniform flow approaching the groin, the bed shear stress was obtained by using the Prandtl tube as a Preston tube (11,14) and by the velocity profile method based on the logarithmic profile. In the region of deflected flow in the vicinity of the groin, where the magnitude as well as the direction of the bed shear stress were unknown, the yaw probe was used as a Preston tube along with the calibration curves obtained by Rajaratnam and Muralidhar (13,15).

Water surface profiles were measured with a water level detector with an accuracy of 0.001 ft (0.3 mm). The data acquisition was facilitated by means of an automatic and programmable system developed for this study (10).

For a selected test discharge, the flume slope and depth were adjusted to establish uniform flow conditions. The velocity distribution in the undisturbed approach flow was measured at about 3.0 ft (0.92 m) upstream of the groin in the center plane of the channel. Then the velocity and bed shear stress in the region of flow deflected by the groin were measured with the yaw probe. (The velocity measurement stations are shown in Fig. 1(b)). Visual observations of the separated flow down-

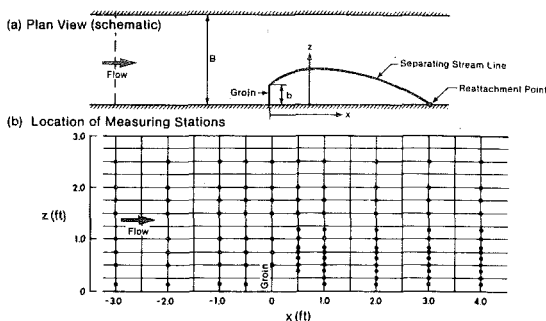


FIG. 1.—Definition Sketch and Measuring Stations

stream of the groin were also made by colour injection. On the whole, 13 experiments were performed as shown in Table 1. In all these experiments, the approaching flow was subcritical with the Froude number approx in the range 0.1–0.3.

## EXPERIMENTAL RESULTS

With reference to Fig. 1(a), the  $x$ -axis is placed along the bed of the channel coinciding with the right sidewall (looking downstream),  $y$  is measured normal to the bed, and  $z$  is the transverse distance from the right side wall to which the groin is attached. The time-averaged turbulent velocities at any point in these three coordinate directions ( $x, y, z$ ) are  $u$ ,  $v$ , and  $w$ , respectively;  $\mathbf{V}$  = the velocity vector. The bed shear stress is denoted by  $\tau_0$  and  $\tau_{00}$  is the value of  $\tau_0$  in the center plane of the undisturbed approach flow. The depth and mean velocity of the approach flow are, respectively,  $y_0$  and  $V_0$ ;  $Q$  = the volumetric flow rate or discharge.

Typical velocity profiles [ $u(y)$ ] measured in the upstream approach section in the centerplane of the channel showed that  $u$  increases linearly with  $\log y$ . The velocity profiles in the region affected by the groin indicated that as the water flows around the groin, the velocity distribution becomes almost uniform (in the vertical direction) near the nose of the groin and in the backward flow region. Downstream from the groin, the profiles showed the formation of a jet close to the bed. The velocity observations indicated that the velocity field in the region deflected by the groin could be analyzed by treating it as a skewed turbulent boundary layer (9). The velocity measurements for experiment A1 for  $x/b = -2, -1, 0, 1, 2, 3$ , and 8 for different values of the transverse distance  $z$  are shown in Fig. 2 in the form of Johnston's polar plots (6,7,12). In these plots, for any location, the  $x$ -component of velocity  $u$  is plotted against the  $z$ -component  $w$ . These plots and similar ones for the other experiments generally showed that in the deflected flow upstream from the groin as well as in the downstream region for the  $x/b$  up to about 1.0, there exists an inner region in which the velocity profiles are collinear and the velocity vectors are in the direction of the bed shear. In the outer layer above the inner layer which terminates at the

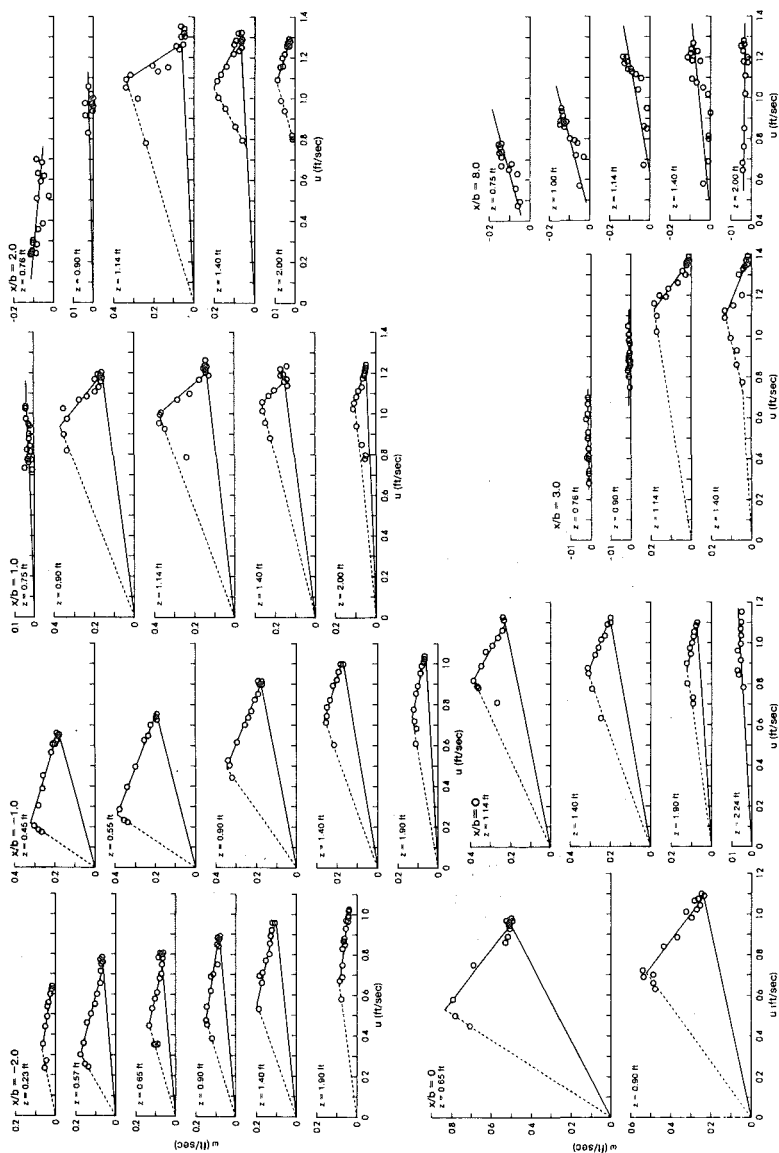


FIG. 2.—Polar Plots in the Deflected Flow Region

TABLE 1.—Details of the Experiments

Experiment (1)	Groin shape (2)	Depth of flow, $y_o$ , in feet (3)	Width of flume, $B$ , in feet (4)	Dis- charge, $Q$ , in cubic feet per second (5)	Mean velocity, $V_o =$ $Q/y_o B$ , in feet per second (6)	Length of groin, $b$ , in feet (7)	Approach bed shear stress, $\tau_{00}$ , in pounds per square foot (8)	Froude Number $F = V_o /$ $\sqrt{gy_o}$ (9)	Nature of bed (10)	Shear stress amplifi- cation, $\tau_{0m}/\tau_{00}$ (11)
A1	thin plate	0.62	3.0	1.6	0.83	0.50	0.0027	0.19	smooth	4.9
A2	thin plate	0.73	3.0	1.6	0.71	0.50	0.0022	0.15	smooth	4.5
A3	thin plate	0.84	3.0	1.6	0.63	0.50	0.0017	0.12	smooth	4.9
A4	thin plate	0.50	3.0	1.6	1.05	0.50	0.0050	0.26	smooth	4.5
A5	thin plate	0.50	3.0	1.2	0.80	0.50	0.0028	0.20	smooth	4.6
B1	thin plate	0.50	3.0	1.6	1.15	0.25	0.0050	0.29	smooth	3.0
B2	thin plate	0.72	3.0	1.6	0.75	0.25	0.0024	0.16	smooth	2.8
B3	thin plate	0.62	3.0	1.6	0.78	0.25	0.0024	0.17	smooth	3.4
C1	thin plate	0.50	3.0	1.58	1.07	0.25	0.0060	0.27	sand paper	5.2
C2	thin plate	0.73	3.0	1.6	0.73	0.50	0.0023	0.15	sand paper	5.3
D1	thin plate	0.72	3.0	1.6	0.75	0.50	0.0060	0.16	hemi- spherical roughness	—
E1	semi- cylindrical	0.50	3.0	1.6	1.05	0.50	0.0047	0.26	smooth	4.2
E2	semi- cylindrical	0.73	3.0	1.6	0.71	0.50	0.0022	0.146	smooth	4.2

Note: 1 ft = 0.305 m; 1 cu ft/sec = 0.028 m<sup>3</sup>/s; 1 psf = 47.9 Pa.

apex of the triangle, the velocity vector increases in magnitude and simultaneously turns continuously away from the bed shear stress until it attains the magnitude and direction of the velocity  $U$  in the upper potential layer. For  $x/b$  greater than about 2.0 and particularly for the verticals with larger values of  $z/b$ , the Johnston triangle begins to deform until the velocity vectors, further downstream, eventually become colinear for the whole depth of flow.

Experimental results for the bed shear stress are shown in Fig. 3(a) for a typical series. These plots and others (not reproduced herein) indicated, in general, considerable increase in bed shear stress  $\tau_0$  near the nose and the immediate neighborhood of the groin. In Fig. 3(a), considering experiment A1 with smooth bed, and  $z = 0.5$  ft. (152 mm), as the nose of the groin is approached,  $\tau_0$  increases rather rapidly from the upstream value of  $\tau_{00} \approx 0.0025$  psf (0.12 kPa) to a maximum of  $\tau_{0m}$  of about 0.013 psf (0.62 kPa) and then decreases rapidly as  $x$  increases, entering into the wake. For  $z$  greater than 0.5 ft (152 mm),  $\tau_{0m}$  assumes decreasing values occurring downstream from the nose. Fig. 3(b) shows a typical contour-type plot for  $\tau_0$  for the neighborhood of the groin.

The features of the velocity distribution downstream from the groin are shown for experiment A1 in Fig. 4(a) for two arbitrarily chosen levels, one for  $y/y_o = 0.03$  and another for  $y/y_o = 0.85$ . Both plots show clearly the backward-flow region behind the groin. At the upper level, the velocity at any  $x$  distance, increases continuously with  $z$ , starting from the backward-flow region, until it merges with the flow speeded up by the constriction caused by the groin. At the lower level, especially for  $x/b = 2$  to 6, a characteristic peak occurs due to bed friction.

As the water flows past the groin, there is a lowering of the water

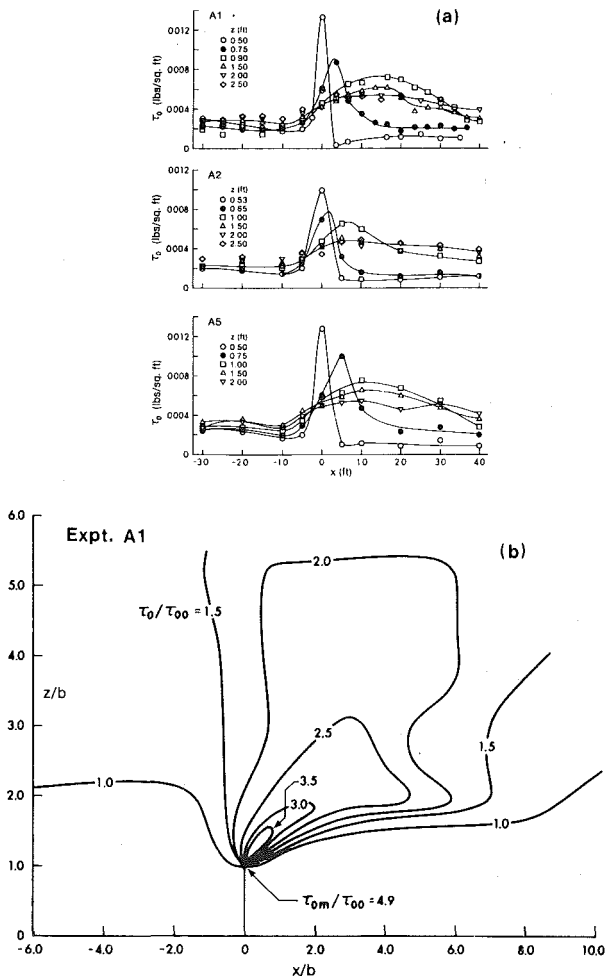


FIG. 3.—Typical Bed Shear Stress Plots

surface at the nose of and behind the groin. The measured profiles showed that for  $z/b = 1.0$ , there is an almost sudden drop near the nose of the groin, but the water surface is almost horizontal upstream and downstream from this drop. The profiles for larger values of  $z$  indicated a gradual fall in the water surface levels.

## ANALYSIS OF EXPERIMENTAL RESULTS

**Approach Flow.**—The velocity profiles  $u(y)$  obtained in the center plane of the approach flow for the A series were plotted in dimensionless form to see whether they satisfy the Karman Prandtl logarithmic law. It was found that, for all five experiments (A1–A5), the data agreed reasonably well with the equation

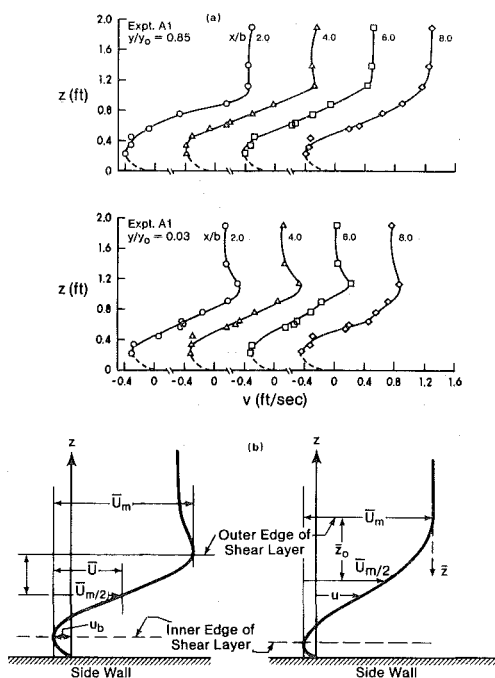


FIG. 4.—Typical Profiles and Definition Sketch of Shear Layer

$$\frac{u}{u_*} = 5.75 \log \frac{y u_*}{\nu} + 5.5 \quad (1)$$

in which  $u_* = \sqrt{\tau_{00}/\rho}$  is the shear velocity;  $\rho$  = the mass density; and  $\nu$  = the kinematic viscosity of water. It was also verified that in series B and E experiments, the dimensionless velocity profiles at the upstream reference station were described by Eq. 1. For these experiments, therefore, the flows were hydrodynamically smooth. The results for one sand-paper (experiment C2) showed that the flow was also hydrodynamically smooth, whereas for the second sand-paper experiment (C1), the flow was in the transition regime from smooth to rough flow. The flow was rough turbulent for the hemispherical roughness.

**The Skewed Boundary Layer.**—In the upstream part of the deflected flow region ( $x$  negative) and for the immediate downstream part up to  $x/b$  of about 1.0, the experimental results showed that the velocity profiles are described by Johnston's polar plots (Fig. 2). If  $y_*$  is the value of  $y$  at the apex of the polar triangle,  $y_* u_*/\nu$  (in which  $u_*$  = the local shear velocity) was found to vary from about 20–300 with all profiles upstream of the groin having a value less than 150. Johnston (7) suggested that the highest value of  $y_* u_*/\nu$  was about 16. However, Hornung and Joubert (6) carried out a more detailed experimental investigation of the three-dimensional boundary layer generated by a circular cylinder, and found that  $y_* u_*/\nu$  ranged up to 150 in the heavily skewed zone upstream from the cylinder. In the inner region in which  $y < y_*$ ,

the velocity data (Fig. 5(a)) are described reasonably well (considering the rather small thickness of this layer) by the logarithmic law of the wall, i.e., Eq. 1.

If  $\alpha$  is the angle through which the upper layer has turned with respect to the approaching flow and  $\beta$  is the angle of the defect velocity with velocity vector of the upper layer (Fig. 5(b)), Johnston (7) and Hornung and Jourbert (6) found that for their skewed boundary layers,  $\beta \approx 2\alpha$ . The results of the present study (Fig. 5(b)) indicate that  $\beta \approx 3\alpha$ . Further, if  $\omega$  is the angle through which the inner layer has turned with reference to the approaching flow (also the angle of bed shear stress), then  $\omega - \alpha$  represents the excess angle of the inner layer with reference to the upper layer. The variation of  $(\omega - \alpha)/\alpha$  with  $z' = (z - b)/b$  is studied in Fig. 5(e). The results indicate that for  $x$  from  $-2.0$  ft– $0.5$  ft ( $-610$  mm– $150$  mm), a mean curve could be drawn through the data and for this mean curve,  $(\omega - \alpha)/\alpha$  decreases from about  $6$  for  $z' \approx -0.5$  to about  $1.0$  for  $z' = 3.0$ .

With reference to Fig. 5(b), if  $U_d$  is the velocity defect at any normal

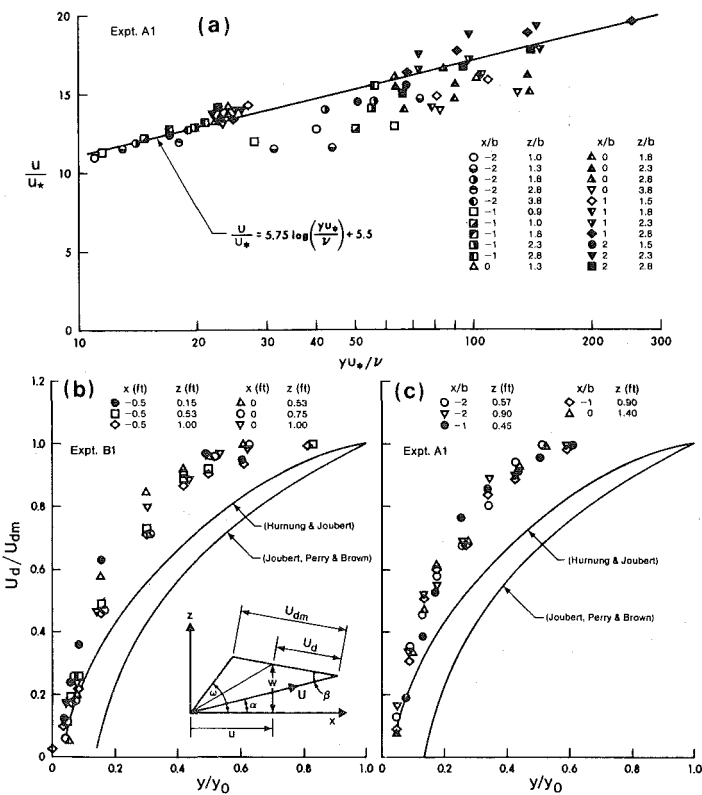


FIG. 5.—Characteristics of the Skewed Boundary Layer: (a) Law of the Wall-Type Velocity Plot; (b and c) Defect Law-Type Plots; (d) Angle of the Velocity Defect; (e) Turning Angle of the Upper Layer; (f) Velocity Scale for Defect Law-Type Plot



distance  $y$  from the bed and if  $U_{dm}$  is the maximum value of  $U_d$ , Horning and Joubert (6) found that in the skewed boundary layer produced by a cylindrical obstacle, the dimensionless velocity defect  $U_d/U_{dm}$  was a function of the dimensionless distance  $y/\delta$  (in which  $\delta$  = the boundary layer thickness). Johnston (8) plotted his data and some others by this

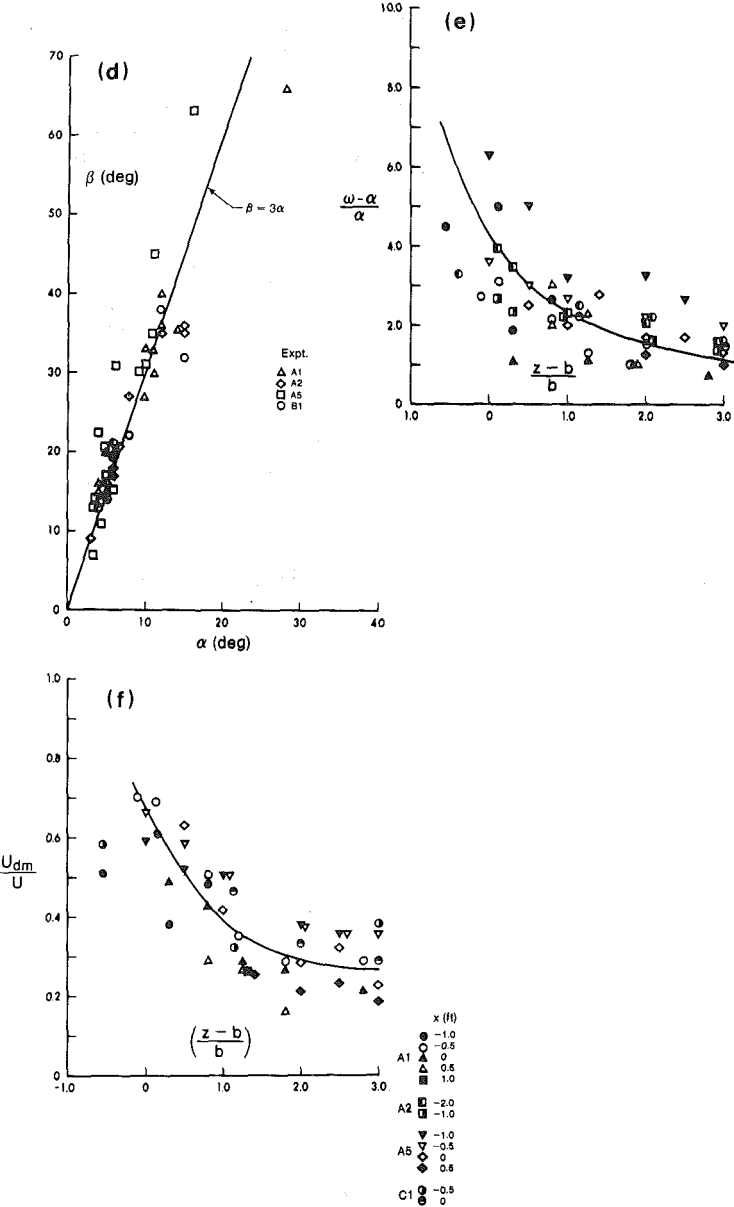


FIG. 5.—Continued

scheme and found that the profiles for each set of data were similar but different from one another and from the curve obtained by Horning and Joubert. The results of experiments A1 and B1 (Fig. 5(b) and (c)) show that the defect profiles for the present study are similar but different from the profiles of these investigations. In Fig. 5(b) and (c), the distance  $y$  from the bed was normalized by the approach flow depth  $y_o$ . The result of a preliminary attempt to predict the defect scale is shown in Fig. 5(f) wherein  $U_{dm}/U$  is plotted against  $z' = (z - b)/b$  for experiments A1 and A5 with the groin length  $b = 6$  in. (152 mm) and for experiment C1 with  $b = 3$  in. (76 mm). Although considerable scatter is evident, it appears possible to draw a mean curve which shows that  $U_{dm}/U$  decreases continuously with  $z'$  from about 0.7 at  $z'/b = 0$  to about 0.27 at  $z'/b = 3.0$ .

**The Upper Potential Flow Layer.**—The flow layer above the region defined by the triangular model in the skewed zone is referred to as the upper potential flow layer. To present the measurements on the characteristics of this upper layer, if  $U_o$  is the velocity of the upper layer in the approaching flow and if  $U$  is its value at any location in the deflected flow region, the variation of  $U/U_o$  against  $x/b$  is shown in Fig. 6(a) for the A series for different values of  $z/b$  where only the mean curves drawn through the experimental points are shown (for clarity). Fig. 6(a) shows that, for  $z/b = 2.0, 3.0$ , and  $4.0$ ,  $U/U_o$  does not decrease below unity, but increases continuously to reach peak values of about 1.45 downstream from the groin.

The variation of  $U/U_o$  with  $x/b$  for various values of  $z/b$  for the 3-in. (76-mm) groin is shown in a consolidated form in Fig. 6(b). From this figure, it is seen that these profiles are similar to those for the 6-in. (152-mm) groin, but the maximum values of  $U/U_o$  are smaller.

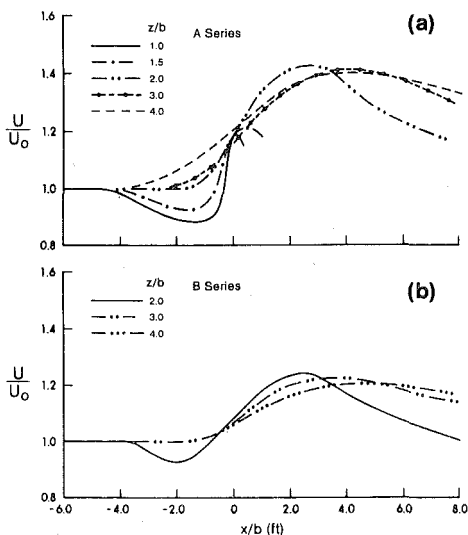


FIG. 6.—Behavior of the Upper Layer (a–d) and the Bed Shear Angle (e)

results of Cunha (2), it appears the results for the 3-in. (76-mm) groin for which  $b/B \approx 1/12$  or  $(B - b)/B = 0.92$  might represent the asymptotic case, i.e., the constriction ratio for which the effect of constriction on the channel flow farther away is negligible.

The variation of the deflection angle of the upper flow layer  $\alpha$  with  $x/b$  for various values of  $z/b$  for the series A experiments is shown in Fig. 6(c) where mean curves have been drawn through the experimental data. For these curves,  $\alpha$  reaches the maximum value of  $\alpha_m$  approximately at the location of the groin and then decreases steadily to assume a small negative value further downstream. It was found that these curves for the 6-in. (150-mm) groin described satisfactorily the  $\alpha$  variation for the 3-in. groin, thereby lending some general importance to the  $\alpha$  variation curves. For the maximum value of the deflection angle,  $\alpha_m$ , occurring approximately at the groin, Fig. 6(d) shows that one curve, could be drawn to describe the results of both the 6-in. (150-mm) and 3-in. (75-mm) groins and that  $\alpha_m$  decreases from about  $20^\circ$  at  $z'/b = 0.5$  to about  $5^\circ$  at  $z'/b = 3.0$ .

**Bed Shear Stress Field.**—The typical bed shear variations presented earlier (Fig. 3) showed that for any given value of  $z/b$ , the bed stress  $\tau_0$  increases from  $\tau_{00}$  to a maximum value of  $\tau_{0m}$  near the groin and then decreases on the downstream side. The values of  $\tau_{0m}/\tau_{00}$  for the different experiments are shown in Table 1. For the A series, this ratio is about 5, whereas for the B series, it is about 3. Thus, the degree of constriction appears to affect the shear stress amplification near the groin. It is difficult to explain the large amplification for experiment C1 and, thus, this large value is discounted as being due to some possible experimental errors. For the 6-in. (152-mm) groin with the sand-paper roughness (se-

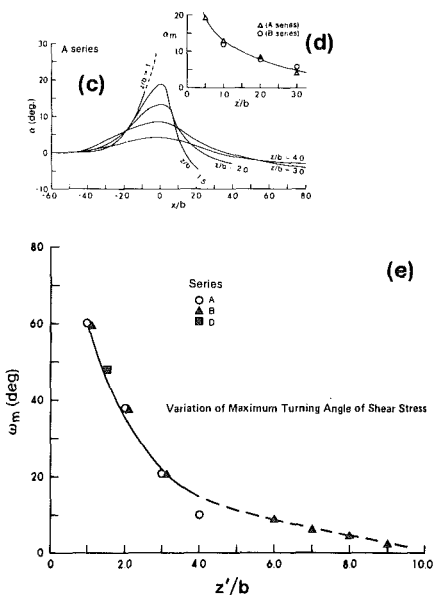


FIG. 6.—Continued

ries C), slightly higher amplification is indicated (Table 1), but since in these experiments, the flow was not fully rough turbulent, no significance can be associated with the higher amplification. Maximum shear stress in experiment D would have provided a better assessment of the effect of roughness, but the necessary data were not obtained due to the intense turbulence, causing instrument vibration at the required location.

The bed shear stress curves shown in Fig. 3 were analyzed for similarity. The shear stress,  $\tau_0$ , was normalized by the approach shear stress  $\tau_{00}$ , and  $x$  and  $z$  were normalized by the groin length  $b$ . The dimensionless plots resembled those of Fig. 3, and are not shown here. However, if  $\Delta\tau_0/\Delta\tau_{Om}$  is plotted against  $x'/b$  wherein  $\Delta\tau_0 = \tau_0 - \tau_{00}$ ,  $\Delta\tau_{Om} = \tau_{Om} - \tau_{00}$ ,  $x' = x - x_m$ ;  $x_m$  = the location of  $\tau_{Om}$ , as shown in Fig. 7(a), it is seen that, on the upstream side of  $x_m$ , a mean curve, could be drawn to describe approximately the data of the present experiments. On the downstream side of the location of  $\tau_{Om}$ , the  $(\Delta\tau_0/\Delta\tau_{Om})$  vs.  $x'/b$  profiles depend for their shape on the value of  $z'/b$ . These upstream and downstream profiles were replotted with  $(\Delta\tau_0/\Delta\tau_{Om})$  vs.  $\eta_r = (x'/b)/[(x'/b)_{1/2}]$  in which  $(x'/b)_{1/2} = (x'/b \text{ at } (\Delta\tau_0/\Delta\tau_{Om}) = 0.5)$ ; as shown in Fig. 7(b), all these profiles could be described by one curve. This curve is described satisfactorily by the exponential equation

$$\frac{\Delta\tau_0}{\Delta\tau_{Om}} = e^{-0.693\eta_r^2} \dots\dots\dots (2)$$

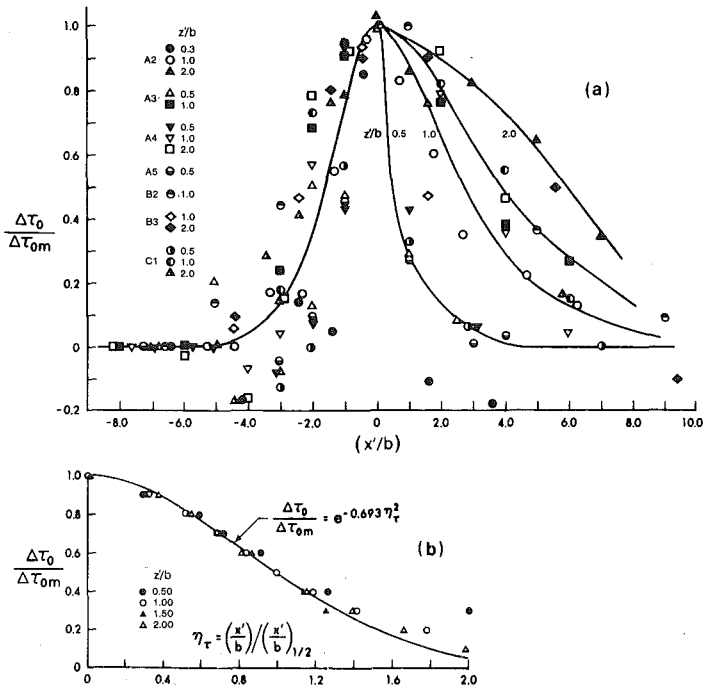


FIG. 7.—Similarity Analysis of the Bed Shear Stress in the Deflected Flow Region

The variation of the length scale  $(x'/b)_{1/2}$  with  $z'/b$  is shown in Fig. 7(c). For the downstream side of  $x_m$ ,  $(x'/b)_{1/2}$  increases with  $z'/b$ , whereas, for the upstream side,  $(x'/b)_{1/2} \approx 1.6$ .

The variation of  $\Delta\tau_{Om}/\tau_{00}$  with  $z'/b$  for the different experiments is studied in Fig. 7(d), which shows that a mean curve could be drawn to represent most of the results and  $\Delta\tau_{Om}/\tau_{00}$  decreases continuously as  $z'/b$  increases from about 4.0 at  $z'/b = 0$  to about 0.75 at  $z'/b = 5.0$ . It would be interesting and useful to perform further experiments to test the validity of this curve for a wider range of  $b/B$ . The variation of  $x_m/b$  with  $z'/b$  is studied in Fig. 7(e). Here again, it appears that a mean curve could be drawn through the data of most experiments, and  $x_m/b$  increases continuously with  $z'/b$  up to  $z'/b \approx 3.0$ , and, for  $z'/b \approx 3.0$ ,  $x_m/b$  approaches an asymptotic value of 3.0.

If  $\omega$  is the angle of the bed shear stress at any point with the longitudinal direction of the undisturbed flow, the variation of  $\omega$  with  $x/b$  for different values of  $z/b$  was studied, and the behavior of  $\omega$  was found to be similar to that of  $\alpha$ . For any value of  $z/b$  (or  $z'/b$ ),  $\omega$  increased from zero to a maximum value of  $\omega_m$  at some value of  $x/b$ , and then decreased continuously to zero with further increase in  $x/b$ . The variation of  $\omega_m$  with  $z'/b$  for three series is shown in Fig. 6(e) in which  $\omega_m$  decreases continuously from  $60^\circ$  at  $z'/b \approx 1$  to about  $2^\circ$  at  $z'/b \approx 9$ .

**The Shear Layer.**—On the downstream side of the groin, the region that lies between the outer plane of the deflected flow, defined approximately by the separating stream line and the side wall on the side of the groin, resembles a shear layer from the configuration of the velocity profiles in that region. The outer edge of the shear layer in any horizontal plane is taken as the point where the velocity either approaches

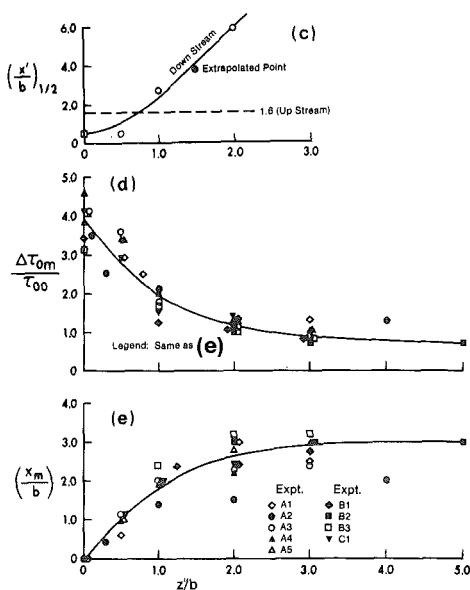


FIG. 7.—Continued

the velocity of the deflected flow or reaches a maximum value (Fig. 4(b)). The inner edge is fixed at the point where the absolute magnitude of the negative velocity reaches the maximum value.

The configuration of the outer boundary of the shear layer for the upper layer is shown in Fig. 8(a) from the results of the A series. This figure also shows the separating stream line computed from the free-stream line theory. The stream line for  $\psi = 0$ , as determined from the actual velocity measurements, is also shown where  $\psi$  is the stream function. Fig. 8(b) shows in addition the range of the outer boundary near the bed for the A series of experiments. From these figures, it could be said that the outer boundary plane of the shear layer through the depth of flow is not vertical; it is tilted towards the backward flow region near the bed. This aspect was also verified visually in the dye tests.

Secondly, the  $\psi = 0$  line, as determined from velocity measurements in the upper layer, is displaced more into the backward flow region than the theoretical free stream line. In general, the theoretical free stream line coincides fairly well with the outer boundary of the shear layer close to the bed for  $x/b$  up to about 8. The theoretical free stream line tends to grow continuously with increasing downstream distance because the theory does not account for the flow interaction in the two zones that the line separates. In reality, the free stream line has two segments as represented in Fig. 8(a) by curve 3. In the first segment, the stream line  $\psi = 0$  grows into the deflected channel flow from the groin nose until the recirculation region behind it attains a maximum width of  $2b$ . The second segment extends from this maximum point to the reattachment

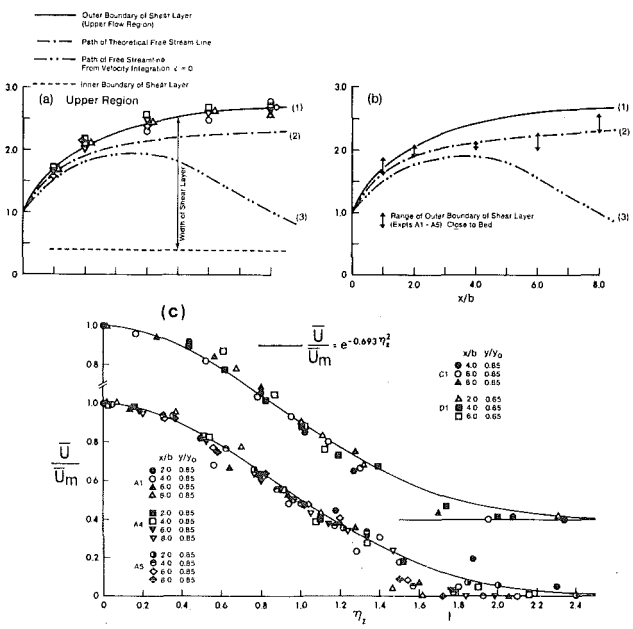


FIG. 8.—Characteristics of the Shear Layer

point at  $x/b \approx 12$ . The length of this recirculation or eddy zone is about six times its maximum width. The dimensions of the eddy zone from this study are consistent with those reported by Francis, et al. (3).

The velocity profiles in the shear layer were tested for similarity by plotting  $\bar{U}/\bar{U}_m$  against  $\bar{z}/\bar{z}_0$  in which  $\bar{U} = u - (u_b)$ ,  $\bar{U}_m$  = the maximum value of  $\bar{U}$ ;  $\bar{z}$  = measured from the outer edge of the shear layer (see Fig. 4(b)); and  $\bar{z}_0 = \bar{z}$  in which  $\bar{U} = 1/2 \bar{U}_m$ . These profiles were picked for two typical levels of  $y/y_0 = 0.85$  and  $0.03$ . The dimensionless plots are shown in Fig. 8(c) for the upper level and Fig. 8(d) for the lower level. Both figures show that the profiles are similar and that the similarity curve is well-described by the exponential curve,  $\bar{U}/\bar{U}_m = e^{-0.693\eta_z^2}$  in which  $\eta_z = \bar{z}/\bar{z}_0$ .

If  $z_i$  is the distance of the inner boundary of the shear layer, the experimental results showed that  $z_i/b \approx 0.4$ . If  $\bar{b}$  = the width of the shear layer, the variation of  $\bar{b}/b$  with  $x/b$  for the upper flow region is shown in Fig. 8(e). The growth of the shear layer for  $x/b$  up to 8.0 is approximately linear, and the shear layer is somewhat wider in the upper region than in the lower region (Fig. 8(f)). The rather limited results of the B series agreed well with the aforementioned results.

The velocity scale  $\bar{U}_m$  for the shear layer for  $x/b$  up to about 8 was approximately constant and  $\bar{U}_m/V_0$ , wherein  $V_0$  is the mean velocity of the approaching flow was equal to 2.06 for the A series and 1.58 for the B series for the upper region. For the lower region, the corresponding values are about 0.75 times the upper region values. To evaluate the variation of  $\bar{U}_m/V_0$  with  $b/B$ , further experiments will have to be made to extend the range of  $b/B$ . If  $|u_b|$  is the magnitude of the maximum value of the backward velocity,  $|u_b|/\bar{U}_m$  was found to be approximately equal to 0.2.

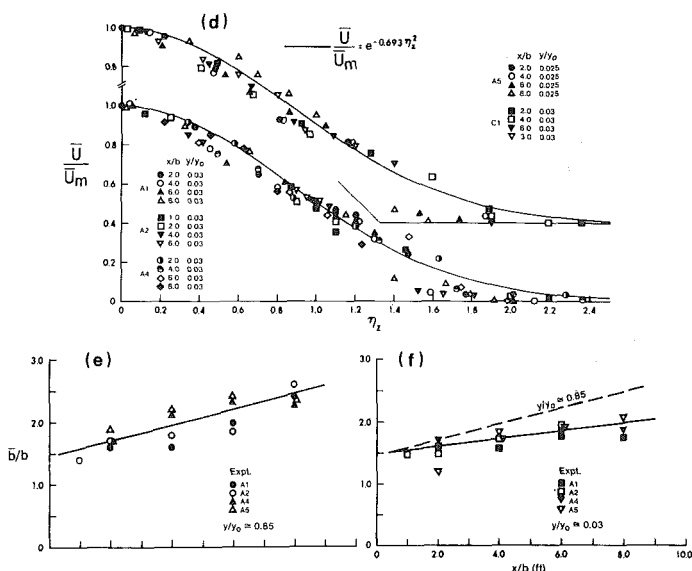


FIG. 8.—Continued

**Effect of Groin Shape.**—In the previous sections, experimental results were presented for the thin plate groines on smooth and rough beds. A limited set of experiments were performed to assess the influence of groin shape (series E experiments). An analysis of these results showed that the characteristics described earlier were present, but the disturbance caused by the cylindrical groin was not as extensive in spatial extent as that for the thin groin. The shear amplification of  $\tau_{0m}/\tau_{00} \approx 4.3$  compared favorably with that for the thin groin of equivalent projection. However, for  $z/b \geq 4$ , the shear stress had reduced to the undisturbed upstream value for all transverse locations. The length of the eddy zone from the point of separation to the reattachment point was found to be only about  $5b$  compared to  $12b$  for the thin groines. These preliminary results indicate the importance of shape particularly for the spacing of groines.

## CONCLUSIONS

This study has shown that when a groin is placed in a channel, it causes a significant disturbance to the flow for a short distance upstream and for a longer distance downstream. The disturbed flow was analyzed by splitting it into a deflected flow region and a shear layer. For the deflected flow region, the skewed turbulent boundary layer model of Johnston was found to be valid. The defect-velocity vectors normalized by the defect velocity vector at the apex of the Johnston's polar plot conformed to the scheme suggested by Hornung and Joubert, and the velocity scale for the defect plot was determined empirically. In the shear layer, the velocity distributions for any horizontal plane were found to be similar. The scales for this similarity profile were evaluated empirically.

The maximum bed shear stress occurred near the groin nose. The shear stress amplification  $\tau_{0m}/\tau_{00}$  varies with  $b/B$ . For the 6-in. (150-mm) groin,  $\tau_{0m}/\tau_{00}$  was about 5, and for the 3-in. (75-mm) groin the same ratio was about 3. All the bed shear stress measurements in the neighborhood of the groin were analyzed effectively using the similarity technique.

## ACKNOWLEDGMENT

The work presented in this paper was performed by B. A. Nwachukwu with the supervision of N. Rajaratnam in the Hydraulics Laboratory of the University of Alberta, Edmonton, and formed part of the doctoral dissertation of B. A. Nwachukwu. The writers are thankful to A. W. Peterson, R. Gitzel, S. Lowell, D. McGowan, A. Muir, B. Klein, J. Lewis, B. Berry, and P. Steffler for their assistance. The writers are also thankful to the Natural Sciences and Engineering Research Council (NSERC) of Canada and the Alberta Dept. of Environment for the financial assistance provided. It should be mentioned that the work contained in the aforementioned dissertation has been issued as a departmental report by the writers in April, 1980.



## APPENDIX I.—REFERENCES

1. Beckstead, G., "Design Considerations for Stream Groines," Technical Dept., Alberta Department of the Environment, Technical Services Div., Edmonton, Alberta, Canada, Oct., 1975.
2. Cunha, L., "Local Scour of Obstacles Protruding from River Banks," thesis presented to the University of Lisbon, at Lisbon, Portugal, in 1971, in partial fulfillment of the requirement for the degree of Doctor of Philosophy.
3. Francis, J., Pattanaik, A., and Wearne, S., "Observations of Flow Patterns Around Some Simplified Groin Structures in Channels," Technical Note 8, *Proceedings*, Institution of Civil Engineers, London, England, Dec., 1968, pp. 829–846.
4. Gill, M. A., "Erosion of Sand Beds Around Spur Dikes," *Journal of Hydraulics Division*, ASCE, Vol. 98, No. HY9, Sept., 1972, pp. 1587–1602.
5. Hollingshead, A., "Boundary Shear Stress Distribution in Open Channel Flow," thesis presented to the University of Alberta, Dept. of Civil Engineering, at Edmonton, Alberta, Canada, in Spring, 1972, in partial fulfillment of the requirement for the degree of Doctor of Philosophy.
6. Hornung, H., and Joubert, P., "The Mean Velocity Profile in Three-Dimensional Turbulent Boundary Layers," *Journal of Fluid Mechanics*, Vol. 15, Part 3, 1963, pp. 368–384.
7. Johnston, J., "On the Three-Dimensional Boundary Layer Generated by Secondary Flow," *Transactions*, American Society of Mechanical Engineers, Series D, Vol. 82, 1960, pp. 233–248.
8. Joubert, P., Perry, A., and Brown, K., "Critical Review and Current Developments in Three-Dimensional Boundary Layers," *Fluid Mechanics of Internal Flow*, Elsevier Publishing Company, Amsterdam, Netherlands, 1967.
9. Nash, J., and Patel, V., *Three-Dimensional Turbulent Boundary Layers*, SBC Technical Books, Sybucon Inc., Atlanta, Scientific and Business Consultants, Atlantic, Ga., 1972.
10. Nwachukwu, B., Gitzel, R., and Peterson, A., "An Application of Microcomputer in the Control, Measurement, and Analysis of Hydraulic Testing," *Proceedings of the Specialty Conference on Computer Application in Hydrotechnical Engineering*, 1978.
11. Patel, V., "Calibration of the Preston Tube and Limitations on its Use in Pressure Gradients," *Journal of Fluid Mechanics*, Vol. 23, Part 1, 1965, pp. 185–208.
12. Perry, A., and Joubert, P., "A Three-Dimensional Turbulent Boundary Layer," *Journal of Fluid Mechanics*, Vol. 22, Part 2, 1965, pp. 285–304.
13. Rajaratnam, N., and Muralidhar, D., "Yaw and Pitch Probes," *Hydraulic Instrumentation Series*, Dept. of Civil Engineering, University of Alberta, Edmonton, Alberta, Canada, Sept., 1967.
14. Rajaratnam, N., and Muralidhar, D., "The Prandtl Tube as a Preston Tube," *Civil Engineering and Public Works Review*, London, England, May, 1968, p. 542.
15. Rajaratnam, N., and Muralidhar, D., "Yaw Probe Used as Preston Tube," Technical Note, *The Aeronautical Journal of the Royal Aeronautical Society*, Vol. 72, Dec., 1968, pp. 1059–60.
16. Zaghoul, N. and McCorquodale, J., "A Numerical Model for Flow Past a Spur-Dike," *Proceedings*, First Canadian Hydraulics Conference, Vol. 1, 1973, pp. 355–368.

## APPENDIX II.—NOTATION

The following symbols are used in this paper:

- $B$  = width of channel;  
 $b$  = length of groin;

$F$	=	Froude number;
$g$	=	acceleration due to gravity;
$k_s$	=	Nikuradse's equivalent sand grain roughness;
$Q$	=	total discharge;
$U$	=	velocity of the upper flow layer in the deflected region;
$\bar{U}$	=	velocity in the shear layer analysis;
$U_d$	=	velocity defect;
$U_{dm}$	=	maximum value of $U_d$ ;
$\bar{U}_m$	=	maximum value of $U$ for shear layer analysis [ $\bar{U} - (u_b)$ ];
$U_o$	=	velocity of the upper flow layer for the approach flow;
$u$	=	time averaged local velocity in $x$ -direction;
$u_*$	=	shear velocity;
$u_b$	=	maximum value of backward velocity;
$V_o$	=	mean approach velocity;
$\mathbf{V}$	=	velocity vector;
$w$	=	transverse component of velocity in $z$ -direction;
$x$	=	coordinate in longitudinal direction;
$x_m$	=	location of maximum shear stress;
$\nu$	=	kinematic viscosity of water;
$\delta$	=	boundary layer thickness;
$\alpha$	=	angle of $U$ with the $x$ direction;
$\tau_{00}$	=	approach bed shear stress;
$\tau_0$	=	bed shear stress in the deflected flow region;
$\tau_{Om}$	=	maximum bed shear stress;
$\Delta\tau_0$	=	$\tau_0 - \tau_{00}$ ;
$\Delta\tau_{Om}$	=	$\tau_{Om} - \tau_{00}$ ;
$\eta_\tau$	=	dimensionless length $(x'/b)/[(x'/b)_{1/2}]$ ;
$\eta$	=	dimensionless length;
$\theta$	=	angle of the velocity vector with $x$ -direction; and
$\omega$	=	angle of the inner layer.